O.P. FEDOROV [1,2,*], A.G. MASHKOVSKY [1], and Ye.L. ZHIVOLUB [2,]**

[1] Space Research Institute of the N.A.S. of Ukraine
and State Space Agency of Ukraine,
40 Glushkov Prosp., Bldg. 4/1, UA-03187 Kyiv, Ukraine

[2] G.V. Kurdyumov Institute for Metal Physics of the N.A.S. of Ukraine,
36 Academician Vernadsky Blvd., UA-03142 Kyiv, Ukraine

*fedorov@ikd.kiev.ua, oleh.fedorov@gmail.com, **zhivolub@imp.kiev.ua

SOLID–MELT INTERFACE STABILITY DURING DIRECTIONAL SOLIDIFICATION: A PHENOMENOLOGICAL THEORY

A mathematical model is developed that makes it possible, within the framework of a single phenomenological approach, to investigate the stability of a planar phase boundary during directional solidification of binary alloy, taking into account the effect of a density change and heat transfer in the solid phase. The study reveals a complex picture of alternating areas of stability and instability, which is sensitive to changes in parameters of growth and temperature gradient at the interface. Areas of instability are formed by the development of a set of disturbances of different frequencies and rates of propagations. As shown, the irreducible liquid-phase flow caused by density change plays a major role in the loss of stability of the solidification front and is realized for perturbations with any wave number $k > 0$.

Keywords: binary alloy, solid–liquid interface, directional solidification, morphological stability, density jump, latent melting heat, dispersion equation.

1. Introduction

The solid–liquid interface stability during directional solidification is of considerable fundamental and practical interest as one of the basic problems of solidification physics [1–3]. This interest is related to the de-

pendence of the crystalline material properties on the morphological features of the crystallization front, as well as to the development of external action technologies on crystallizing melts. The problem of interface stability is also important in the development of new methods of space material sciences [4, 5].

An adequate physical description of directional solidification requires a coherent solution of three interrelated problems: three-dimensional hydrodynamic problem, heat and mass transfer and two-dimensional morphological stability one [2]. In general terms, meeting the conditions of these three tasks together is a major challenge, so substantial simplifications are introduced when considering real crystallization [1, 3, 6].

The theoretical study of interface stability typically uses the classical approach of Mullins and Sekerka, based on the analysis of the evolution of infinitesimally small perturbations of the planar front [6]. It follows from the analysis that the shape of the boundary is stable with respect to any small perturbations when the pulling rate is below of some critical value (under a fixed temperature and concentration gradient at the interface). Otherwise, crystallization front loses stability, and a sequence of unstable structures (nodes, cells, dendrites) appeared.

It is known that taking into account real crystallization factors ca change the stability areas identified in the theory [6]. For example, various effects of melt flow on interface stability have been detected theoretically and experimentally: stimulation and suppression of perturbations by melt flow, coupled convective–morphological instability, traveling waves, *etc.* [7–13]. The analysis of the interface stability in the conditions of lateral melt flow has demonstrated a complicated pattern of alternation of stability areas, which is substantially dependent on the flow rate [13].

However, it should be noted, that the above mentioned works (including the linear model [6] as well as the model in Ref. [13]) have certain limitations, as they ignore the effect of density change during crystallization and the resulting melt flow as well as the effect of heat transfer through the solid phase. The above-mentioned factors are usually neglected because of their small effect in comparison with the main factor in action, namely, constitutional melt supercooling. However, without proper analysis, this simplification does not appear to be physically justified. For example, a number of works on dendritic growth theory, eutectic crystallization, and crystal growth kinetics have shown the significant role of density change during crystallization [14–18].

This paper is dedicated to the construction of a phenomenological theory of stability, in which it is possible to compare above mention acting physical factors during directional crystallization in a two-component system. The study of the morphological stability is carried out

using the phenomenological approach in the framework of continuum mechanics in planar geometry. Furthermore, the boundary value problem of directional solidification under stationary conditions is solved, and then the eigenvalues of the boundary value problem, formulated for infinitely small perturbations of the stationary process, are determined. This approach allows studying morphological stability for perturbations with any wave number $k > 0$.

2. Problem Statement, Basic Equations of the Model

Two-dimensional scheme of a stationary directional solidification of a binary melt is considered, as shown in Fig. 1: positive direction of the co-ordinate axes: Y — from the reader, X — to the right. A binary melt is located in the upper half-plane ($Z > 0$), and a solid phase is in the lower one ($Z < [0, \infty]$. The crystallization front lies in the plane X, Y ($Z = 0$) at $\forall t \in [0, \infty]$. The laboratory co-ordinate system (X', Y', Z') is connected to the ampoule and moves in the positive direction of the Z'-axis with the interface velocity (solidification rate) w. Co-ordinate transformations are determined by the following ratios:

$$x = x', \ y = y', \ z = z' - wt.$$

It is assumed that w modulo coincides with the pulling rate of the ampoule $|\mathbf{V}so|$ (Fig. 1). Here and further, all parameters are represented in a dimensionless form. The characteristic values of the parameters under converting the equations to a dimensionless form and the values of the physical parameters of the object under study are given in Appendixes 1–3.

In the absence of external forces, the general type of the equation describing the heat and mass transfer in the area divided by the interface is presented in Appendix 1.

The difference between the temperatures of the liquid and solid phases and the temperature of the crystallization front θ_l and θ_S will be called henceforth simply the temperature of the stationary state of liquid and solid phases respectively. The type of dimensionless complexes Re, P_l, P_s and others is given in Appendix 1.
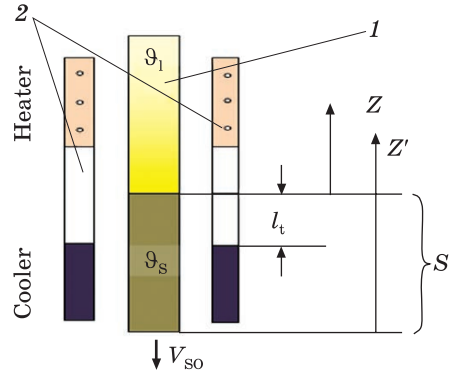
In the set of equations and boundary conditions (A1.1)–(A1.13), the variables are represented as follows:

$$v_y(y,z,t) \to 0 + \varepsilon v_y(y,z,t), \ v_z(y,z,t) \to (1-\rho)\cdot w + \varepsilon v_z(y,z,t),$$

$$p(y,z,t) \to p_0(z) + \varepsilon p(y,z,t), \ T_l(y,z,t) \to \theta_l(z) + \varepsilon T_l(y,z,t),$$

$$C(y,z,t) \to J(z) + \varepsilon C(y,z,t), \ T_s(y,z,t) \to \theta_s(z) + \varepsilon T_s(y,z,t),$$

$$h(y,t) \to \varepsilon h(y,t),$$

where ε is infinitesimal quantity.

After substitution of the above decompositions in (A1.1)–(A1.10), in zero approximation relative to ε, one obtains a set of equations de-

Fig. 1. Scheme of the directional solidification process. Here, *1* is ampoule containing a binary melt; *2* is device consisting of heater and cooler; ϑ_l is heater temperature; ϑ_s is cooler temperature; *S* is interface position; l_t is distance of the interface from the cooler; *Vso* is velocity vector of the ampoule relative to heater/cooler device

scribing in flat geometry the stationary process of directional solidification schematically presented in Fig. 1:

$$\frac{dV_z}{dz} = 0, \tag{1}$$

$$\frac{d^2\theta_l}{dz^2} + P_l \cdot \rho \cdot w \frac{d\theta_l}{dz} = 0, \tag{2}$$

$$\frac{d^2J}{dz^2} + \rho \cdot w \frac{dJ}{dz} = 0, \tag{3}$$

$$\frac{d^2\theta_s}{dz^2} + P_s \cdot \rho \cdot w \frac{d\theta_s}{dz} = 0, \tag{4}$$

where V_z is the melt flow rate along *Z*-axis, *J* is mass fraction of impurity in alloy.

According to (A1.6)−(A1.10), the solutions of the set of equations of the stationary process (1)−(4) meet following boundary conditions:

$$\theta_l(\infty) = \theta_l, \ J(\infty) = 1, \tag{5}$$

$$V_z(0) = (1 - \rho) \cdot w, \tag{6}$$

$$\theta_l(0) = \theta_s(0), \ \theta'_s(0) - \chi \cdot \theta'_l(0) = \Lambda^* \cdot \rho \cdot w, \tag{7}$$

$$J'(0) + (1 - k) \cdot \rho \cdot w \cdot J(0) = 0, \tag{8}$$

$$\theta_s(-l_t) = \vartheta_s, \ l_t > 0, \tag{9}$$

where ϑ_l and ϑ_s are the temperature at infinity in the liquid phase and temperature at some isotherm at $z = -l_t$ in the solid phase. They can be conventionally assumed to be heater and cooler temperatures respectively; $V_z(z) = $ const is the velocity of melt flow normal to the unperturbed interface (due to the density change), ρ (>1) is the ratio of density of solid and liquid phases, Λ^* is the modified latent melting heat as determined by the ratio

$$\Lambda^* = \Lambda - Ew \cdot (U_s(0) - U_l(0)), \tag{10}$$

where Λ is the latent heat of melting, U_s is internal energy of the solid phase, U_l is internal energy of the liquid phase. The prime $'$ in boundary conditions (7) and (8) and hereinafter refers to the differentiation by variable z.

As follows from the ratio (A1.13), the phenomenological relation at the surface $z = 0$ must also be met:

$$\theta_l(0) = -B_m \cdot J_m(0), \tag{11}$$

where $J_m(0)$ is the molar fraction of the impurity at the interface (normalized to unit at $z = \infty$)). The ratio (A1.21) states the relation of molar fraction of impurity $J_m(z)$ with mass fraction $J(z)$.

Taking into account Eq. (11), the solution of the boundary problem (1)–(9) takes the following form: $J'(0) + (1 - k) \cdot \rho \cdot w \cdot J(0) = 0$

$$V_z(z) = (1 - \rho) \cdot w, \tag{12}$$

$$\theta_l(z) = \vartheta_l \cdot (1 - e^{-P_l \cdot \rho \cdot w \cdot z}) + \vartheta_0 \cdot e^{-P_l \cdot \rho \cdot w \cdot z}, \tag{13}$$

$$J(z) = 1 + \frac{(1 - \kappa) \cdot e^{-\rho \cdot w \cdot z}}{\kappa}, \tag{14}$$

$$\theta_z(z) = \frac{\vartheta_0 \cdot (e^{-P_s \cdot w \cdot z} - e^{P_s \cdot w \cdot l}) + \vartheta_s \cdot (1 - e^{-P_s \cdot w \cdot z})}{1 - e^{P_s \cdot w \cdot l}}, \tag{15}$$

where

$$\vartheta_0 = -B_m \cdot J_m(0). \tag{16}$$

Because of the condition of conservation the energy density flux through the crystallization front (7) and the phenomenological ratio (11), it follows from the solutions (12)–(15) that the temperatures ϑ_l, ϑ_s (Fig. 1) must satisfy the ratio

$$\theta_l = \frac{P_s \cdot [\vartheta_s - \vartheta_0]}{\chi \cdot P \cdot_l (1 - e^{P_s \cdot w \cdot l_t})} - \frac{\Lambda^*}{\chi \cdot P} + \vartheta_0$$

or more suitable for analysis

$$\tau = \ln \left[1 - \frac{P_s \cdot (\vartheta_s - \vartheta_0)}{\chi \cdot P_l \cdot (\vartheta_l - \vartheta_0) + \Lambda^*} \right], \tag{18}$$

where

$$\tau = P_s \cdot w \cdot l_t, \tag{19}$$

l_t defines the position of the crystallization front relative to the cooler (Fig. 1), P_l and P_s are Peclet numbers for liquid and solid phases, respectively.

From (18), it can be seen that, for fixed boundary temperatures of heater ϑ_l and cooler ϑ_s (at $z = \infty$ and $z = -l_t$, respectively; Fig. 1), param-

eter τ is constant. Thus, the velocity w determines the position of the crystallization front relative to the heater and cooler (Fig. 1).

Let us enter

$$\zeta = \frac{P_s \cdot (\vartheta_0 - \vartheta_s)}{\vartheta_0 \cdot (1 - \kappa) \cdot (1 - e^{\tau})}, \tag{20}$$

through which the temperatures of the heater ϑ_l and the cooler ϑ_s are defined as follow:

$$\vartheta_l = \vartheta_0 \cdot \left[1 - \frac{(1 - \kappa) \cdot \zeta}{\chi \cdot P_l} \right] - \frac{\Lambda^*}{\chi \cdot P_l}, \tag{21}$$

$$\vartheta_s = \vartheta_0 \cdot \left[1 - \frac{(1 - \kappa) \cdot (1 - e^{\tau}) \cdot \zeta}{P_s} \right]. \tag{22}$$

3. Study of Interface Stability

To study the stability of the phase boundary, let us consider the infinitesimal perturbation of stationary variables in the set of Eqs. (A1.1)–(A1.13). Based on the above-introduced representations of variables in the form of extensions of infinitesimally small parameter ε, in the first approximation, we get:

$$\frac{\partial v_y}{\partial t} - \rho \cdot w \frac{\partial v_y}{\partial z} = -\frac{\partial p}{\partial x} + \frac{1}{Re} \left(\frac{\partial^2 v_y}{\partial y^2} + \frac{\partial^2 v_y}{\partial z^2} \right), \tag{23}$$

$$\frac{\partial v_z}{\partial t} - \rho \cdot w \frac{\partial v_z}{\partial z} = -\frac{\partial p}{\partial x} + \frac{1}{Re} \left(\frac{\partial^2 v_z}{\partial y^2} + \frac{\partial^2 v_z}{\partial z^2} \right), \tag{24}$$

$$\frac{\partial v_y}{\partial y} + \frac{\partial v_z}{\partial z} = 0, \tag{25}$$

$$\frac{\partial T_l}{\partial t} + \frac{\partial \theta}{\partial z} v_z - \rho \cdot w \frac{\partial T_l}{\partial z} = \frac{1}{P_l} \left(\frac{\partial^2 T_l}{\partial y^2} + \frac{\partial^2 T_l}{\partial z^2} \right), \tag{26}$$

$$\frac{\partial C}{\partial t} + \frac{\partial J}{\partial z} v_z - \rho \cdot w \frac{\partial C_l}{\partial z} = \frac{\partial^2 C}{\partial y^2} + \frac{\partial^2 C_l}{\partial z^2}, \tag{27}$$

$$\frac{\partial T_s}{\partial t} - w \frac{\partial T_s}{\partial z} = \frac{1}{P_s} \left(\frac{\partial^2 T_s}{\partial y^2} + \frac{\partial^2 T_s}{\partial z^2} \right), \tag{28}$$

where v_y and v_z are perturbations of the velocity component in the direction of the axes Y and Z, respectively; p is perturbation of pressure; T_l, C are perturbations of temperature and mass fraction of impurities in the liquid phase, respectively; T_s is perturbation of temperature in the solid phase; P_l, P_s are Peclet numbers for liquid and solid phases, respectively.

The solutions of the set of Eqs. (23) to (28) shall meet the boundary conditions:

$$v_y(y, \infty) = v_z(y, \infty) = T_l(y, \infty) = C(y, \infty) = 0, \tag{29}$$

$$v_z(0) = (1 - \rho)\frac{\partial h}{\partial t}, \tag{30}$$

$$Mp \cdot Re \cdot \left[\frac{\partial \alpha}{\partial C}\left(J'(0)\frac{\partial h}{\partial y} + \frac{\partial C}{\partial y}\right) + \frac{\partial \alpha}{\partial T}\left(\theta_l'(0)\frac{\partial h}{\partial y} + \frac{\partial T_l}{\partial y}\right)\right] +$$

$$+ \frac{\partial v_y}{\partial z} + \frac{\partial v_z}{\partial y} - Re \cdot \rho \cdot w \cdot v_y = 0, \tag{31}$$

$$\frac{\partial T_s}{\partial z} - \chi\frac{\partial T_l}{\partial z} + [\theta_s''(0) - \chi \cdot \theta_l''(0)] \cdot h - \rho \cdot w \cdot E_w \times$$

$$\times \left\{\frac{\partial U_l}{\partial T} \cdot T_l - \frac{\partial U_s}{\partial T} \cdot T_s + \left[\frac{\partial U_l}{\partial T} \cdot \theta_l'(0) - \frac{\partial U_s}{\partial T} \cdot \theta_s'(0)\right] \cdot h\right\} +$$

$$+ \rho \cdot \left\{\Lambda + h \cdot \left[\frac{\partial U_l}{\partial T} \cdot \theta_l'(0) - \frac{\partial U_s}{\partial T} \cdot \theta_s'(0)\right]\right\} - \rho \cdot \Lambda^* \cdot \frac{\partial h}{\partial t} = 0, \tag{32}$$

$$T_l = T_s + [\theta_s'(0) - \theta_l'(0)] \cdot h, \tag{33}$$

$$T_l = -\{B_m \cdot C_m + B_s \cdot \alpha \cdot (\partial^2 h/\partial y^2) + [\theta_l^{\uparrow\prime}(0) + B_m \cdot J_m^{\uparrow\prime}(0)]h\}, \tag{34}$$

$$\frac{\partial C}{\partial z} + (1 - \kappa) \cdot \rho \cdot w \cdot C + (1 - \rho \cdot \kappa)J(0)\frac{\partial h}{\partial t} +$$

$$+ [(1 - \kappa) \cdot \rho \cdot w \cdot J'(0) + J''(0)] \cdot h - J(0) \cdot v_z = 0, \tag{35}$$

$$T_s(y, -\infty) = 0, \tag{36}$$

where $h(y, t)$ is the perturbation of the solidification front, Mp, Re, E_w, B_m, B_s are the dimensionless complexes given in (A1); $\alpha(C, T)$ is the dimensionless density of free energy at the interface as a function of concentration and temperature, χ is the ratio of heat conductivity coefficients of liquid and solid phases, Λ^* is modified latent heat of melting (10). The relationship between the $J'_m(0)$ and $J'(0)$, the molar fraction perturbation $C_m(y, z, t)$ and the mass fraction perturbation $C(y, z, t)$ are defined by the relationship (A1.23) and (A1.22), respectively.

Note that the boundary conditions (30)–(35) are obtained from the general conditions for the conservation of flux on the perturbed discontinuity surface (A1.6)–(A1.12) with subsequent assignment to the unperturbed interface $z = 0$.

In the expressions (23)–(36), the transition to amplitude representation is made. In Eqs. (23)–(28) and boundary conditions (29)–(36), the stream function is entering as follows:

$$v_y = \frac{\partial \psi}{\partial z}, \quad v_z = -\frac{\partial \psi}{\partial y}, \tag{37}$$

and the desired variables are represented as

$$[\psi(y, z, t),\, p(y, z, t),\, T_l(y, z, t),\, C(y, z, t),\, T_s(y, z, t),\, h(y, t)]^T =$$

$$= [\varphi(y, t),\, \Pi(z),\, T_l(z),\, C(z),\, T_s(z),\, \eta]^T \cdot e^{i \cdot (k \cdot y\, -\, \omega \cdot t)}, \tag{38}$$

where k is the wavenumber, ω is the complex frequency.

Substituting (37) and (38) into (23)–(36) and excluding the pressure perturbation amplitude $\Pi(z)$ in Eqs. (23) and (24), we obtain a three-point boundary value problem for the perturbation amplitudes:

(a) differential equations

$$\varphi^{IV} + \mathrm{Re} \cdot \rho \cdot w \cdot \varphi^{III} - (2k^2 - \mathrm{Re} \cdot i\omega) \cdot \varphi^{II} - k^2 \cdot \mathrm{Re} \cdot \rho \cdot w \cdot \varphi^{I} + \tag{39}$$

$$+ T_l^{II} + P_l \cdot \rho \cdot w \cdot T_l^{I} - (k^2 - P_l \cdot i\omega) \cdot T_l = -i \cdot k P_l \cdot \theta_l' \cdot \varphi, \tag{40}$$

$$C^{II} + \rho \cdot w \cdot C^{I} - (k^2 - i\omega) \cdot C = -i \cdot k \cdot J' \cdot \varphi, \tag{41}$$

$$T_s^{II} + P_s \cdot w \cdot T_s^{I} - (k^2 - P_s \cdot i\omega) \cdot T_s = 0; \tag{42}$$

(b) boundary conditions

$$\varphi(\infty) = \varphi'(\infty) = T_l(\infty) = C(\infty) = 0, \tag{43}$$

$$k \cdot \varphi(0) - (1 - \rho) \cdot \omega \cdot \eta = 0, \tag{44}$$

$$\varphi''(0) - \mathrm{Re} \cdot \rho \cdot w \cdot \varphi'(0) - i \cdot k \cdot \varphi(0) + i \cdot k \cdot \mathrm{Re} \cdot Mp \cdot (\alpha_{\downarrow}c \cdot C + \alpha_{\downarrow}(T) \cdot T_{\downarrow}l + \tag{45}$$

$$+ T_s'(0) - \chi \cdot T_l'(0) + \rho \cdot w \cdot E_w \cdot (c_{vs} \cdot T_s - c_{vl} \cdot T_l) + [\theta_s''(0) - \chi \cdot \theta_l''(0) +$$

$$+ \rho \cdot w \cdot E_w \cdot (c_{vs} \cdot \theta_s'(0) - c_{vl} \cdot \theta_l'(0)) + i \cdot \rho \cdot w \cdot \Lambda^*] \cdot \eta = 0, \tag{46}$$

$$T_l(0) - T_s(0) + (\theta_l'(0) - \theta_s'(0)) \cdot \eta = 0, \tag{47}$$

$$T_l(0) + B_m \cdot C_m(0) + [(\theta_l'(0) + B_m \cdot J_m'(0) - \alpha B_s \cdot k^2] \cdot \eta = 0, \tag{48}$$

$$C_l'(0) + (1 - \kappa) \cdot \rho \cdot w \cdot C_l(0) + [(1 - \kappa) \cdot \rho \cdot w \cdot J_m'(0) + J_m''(0) -$$

$$- i \cdot \omega \cdot (1 - \rho \cdot \kappa) \cdot J(0)] \cdot \eta + i \cdot k \cdot \varphi = 0, \tag{49}$$

$$T_s(-\infty) = 0. \tag{50}$$

Here, it is assumed that the free energy of the interface $\alpha(C, T)$ is a linear function of concentration and temperature, and the values α_c, α_T in Eq. (45) are

$$\alpha_C = \left(\frac{\partial \alpha}{\partial C} \right)_{T = \mathrm{const}}, \quad \alpha_T = \left(\frac{\partial \alpha}{\partial T} \right)_{C = \mathrm{const}},$$

c_{vl} and c_{vs} are specific heat capacities for liquid and solid phases, respectively.

4. Solving a Boundary Problem;
Hierarchy of Considered Models

The coefficients of the set of Eqs. (39)–(42) are functions of the variable z and contain exponents; therefore, the general solution of this system was sought in the form of an expansion in terms of exponents. It was assumed that

$$Re \ll 1, \ P_l \ll 1, \ P_s \ll 1. \tag{51}$$

The general solution found for the set (39)–(42) satisfying the boundary conditions (43) and (50) is

$$\varphi(z) \cong (C_1^\varphi + C_2^\varphi \cdot z)\, e^{-k \cdot z}, \tag{52}$$

$$C(z) \cong C^c \cdot f_1^c(z)\, e^{-\lambda_2 z} + [C_1^\varphi \cdot f_2^c(z) + C_2^\varphi \cdot f_3^c(z)]\, e^{-(w+k)z}, \tag{53}$$

$$T_l(z) \cong C^t \cdot f_1^t(z)\, e^{-\lambda_2 z} + [C_1^\varphi \cdot f_2^t(z) + C_2^\varphi \cdot f_3^t(z)]\, e^{-(w+k)z} \tag{54}$$

$$T_s(z) \cong C^s \cdot e^{-\lambda_3 z}, \tag{55}$$

where C_1^φ, C_2^φ, C^c, C^t, C^s are arbitrary constants. Appendix 2 represents the types of functions in Eqs. (53), (55) and λ_i ($i = 1, 2, 3$).

Applying the solutions (52)–(55) to boundary conditions (44)–(49) results in a uniform linear set of algebraic equations:

$$\mathbf{A}(k,\Omega)\, x = 0, \ x^T = [C^c, \ C^s, \ C^t, \ \eta, \ C_1^\varphi, \ C_2^\varphi], \tag{56}$$

where

$$\Omega = \sqrt{w^2 + 4\,(k^2 - i\omega)}. \tag{57}$$

The set (52) will have a nontrivial solution, if the determinant of the matrix $\mathbf{A}(k,\Omega)$ satisfies the condition

$$\left|\mathbf{A}(k,\Omega)\right| = 0. \tag{58}$$

Equation (58), taking into account (57), associates the wave number k with the complex frequency ω. This type of equation is traditionally called the dispersion equation. From the determinant of Eq. (58), one can obtain a dispersion equation in the form of a polynomial of degree n with respect to the variable Ω:

$$\sum_{j=0}^{n} Q_{n-j} \cdot \Omega^{n-j} = 0. \tag{59}$$

The roots of the polynomial (59) together with ratio (57) give the dependence of the natural complex frequencies ω of the boundary value problem (39)–(50) on the wave number and the physical parameters of the process. The sign and the numerical value of the imaginary part of the complex frequency ω determine the increase rate of perturbations amplitudes over time ('+' increment) or ('–' decrement). Using (38) and (57), one can obtain a relationship linking the imaginary part of the i-th

natural frequency with the *i*-th root of the dispersion Eq. (59):

$$\delta_i(k, w; \Delta) = \frac{Re(\Omega_i^2)}{4} - k^2 - \frac{p^2 w^2}{4}, \quad i \in \{1, \ldots, n\}, \tag{60}$$

where Δ is the set of physical parameters that define a process. Stability condition for a *i*-th degree of freedom at given values k, w, Δ is determined by the ratio

$$\delta_i(k, w, \Delta) < 0. \tag{61}$$

If the ratio (61) holds for all degrees of freedom $i \in \{1, \ldots, n\}$ on a given set $\{k, w; \Delta\}$, the object is stable on this set. If, for at least one value of $i_1 \in \{1, \ldots, n\}$, $\delta_{i1}(k, w; \Delta) > 0$ and fixed parameters k, w, Δ, the object is unstable at these parameters. Turning (61) into equality $\delta_i(k, w; \Delta) = 0$, in general, one gives some area of neutral stability in the area of parameters $\{k, w, \Delta\}$. In the case of two parameters, for example (k, w), a neutral stability curve is appeared on the corresponding plane separating the stability and instability areas.

If the number of degrees of freedom of an object under study, $n > 1$, it seems advisable to introduce a generalized spectral characteristic of the increase index (increment) as follows:

$$\delta_m(k, w; \Delta) = \max_{i \in (1, \ldots, n)} \delta_i(k, w; \Delta). \tag{62}$$

Then, the sign of $\delta_m(k, w; \Delta)$ will be guaranteed to determine the stability or instability of the object.

The order *n* of the dispersion Eq. (59) is determined by the number of critical physical factors that are used in the mathematical modelling of the object under study. Note that, in general, an object with spatially distributed parameters has an infinite number of degrees of freedom (eigenvalues), $n = \infty$. Meanwhile, the number of eigenvalues corresponding to instability can be both finite and infinite. Next, to assess the criticality of certain factors for the stability of the crystallization front, let us consider some hierarchy of mathematical models: from the simplest to quite complex.

The simplest mathematical model of directional solidification includes differential equations of heat transfer in the liquid phase (26), transfer of impurity in the liquid phase (27), boundary conditions (29), (33), (34) and a condition for impurity flow continuity when crossing the phase boundary (35). Due to the approximation considered, one put $v_z(0) = 0$ in (35). This model is close to that considered by Mullins and Sekerka [6].

If, in the above ratios, we pass to the amplitude representation (38), it can be obtained the solutions of equations (26), (27) of the form (53), (54) at zero values of C_1^φ and C_2^φ. After substitution of the obtained solutions into boundary conditions, we get a system of three linear equations of the form (56). The determinant of the matrix of this system leads to a second-order dispersion equation

$$Q_2 \cdot \Omega^2 + Q_1 \cdot \Omega + Q_0 = 0, \tag{63}$$

where

$$Q_2 = -B_w \cdot \mu_1, \tag{64}$$

$$Q_1 = 2 \cdot [\theta_s'(0) + B_w \cdot J'(0) - B_s \cdot k^2], \tag{65}$$

$$Q_0 = \mu_2 \cdot Q_1 + B_w \cdot [\mu_1 \cdot (\rho \cdot w + 2 \cdot k)^2 + 4 \cdot \mu_0], \tag{66}$$

$$\mu_\downarrow 0 = (1 - \rho \cdot \kappa) \cdot k \cdot \rho \cdot w \cdot J(0) + (1 - \kappa) \cdot \rho \cdot w \cdot J^\uparrow{}'(0) + J^\uparrow{}''(0), \tag{67}$$

$$\mu_1 = -(1 - \rho \cdot \kappa) \cdot J(0), \tag{68}$$

$$\mu_2 = -\rho \cdot w \cdot (3 - 2 \cdot \kappa - Re). \tag{69}$$

The functional relationship between B_w and B_m is represented by the ratio (A1.24). Thus, the study of the stability of the crystallization front in this case is reduced to the computation of the roots of the second-order polynomial (dispersion) Eq. (63) with the subsequent determination of the spectral characteristic of the generalized increment $\delta_m(k)$ (62) in some area of allowable values $\{k, w; \Delta\}$. The approximation considered is called model #1.

In the next, more complex mathematical model (#2), in addition to the ratios (26), (27), (29), (33)–(35), one considers the heat transfer in solid phase, equation (28). This will satisfy the condition of conservation of perturbed energy flux density (32) as well as the condition (36). Then, running sequentially the same operations as in the previous model, one gets the variance equation of the form

$$Q_3 \cdot \Omega^3 + Q_2 \cdot \Omega^2 + Q_1 \cdot \Omega + Q_0 = 0, \tag{70}$$

where

$$Q_3 = -\mu_4,$$

$$Q_2 = \mu_1 \cdot B_w \cdot (a_{11} + a_{12}) - \mu_4 \cdot \mu_2,$$

$$Q_1 = \mu_4 \cdot (\rho \cdot w + 2 \cdot k)^2 + 4 \cdot a_{12} \cdot (a_{24} - a_{34}) - 2 \cdot a_{11} \cdot a_{34},$$

$$Q_0 = \mu_2 \{2 \cdot [\mu_4 \cdot (\rho \cdot w + 2 \cdot k)^2 + 4 \cdot \mu_3] + 4 \cdot a_{12} \cdot (a_{24} - a_{34}) -$$
$$- 2 \cdot a_{11} \cdot a_{34}\} - B_w \cdot (a_{11} + 2 \cdot a_{12}) \cdot [\mu_3 \cdot (\rho \cdot w + 2 \cdot k)^2 + 4 \cdot \mu_0],$$

$$a_{11} = 2 \cdot k \cdot \chi - \rho \cdot w \cdot [2 \cdot E_w \cdot c_{vl} - \chi \cdot (P_l - Re)],$$

$$a_{12} = k + \frac{1}{2} \cdot w \cdot (P_s + 1 \cdot \rho \cdot E_w \cdot c_{vs}),$$

$$\mu_3 = -k \cdot \rho^2 \cdot w \cdot \Lambda^* + \theta_s(0)^{-\chi\theta\_l^r} - \rho \cdot w \cdot E_w \cdot (c_{vl} \cdot \theta_l'(0) - c_{vs} \cdot \theta_s'(0)),$$

$$\mu_4 = \rho \cdot \Lambda^*.$$

Compared to the previous model (63), the energy exchange at the phase boundary is considered, which includes the latent melting heat Λ

(10). As a result, model #2 increased the order of the obtained disper-sion Eq. (70): $n = 3$.

Finally, consider an even more complex model #3, which, in addi-tion to the physical factors included in the models #1and #2 (63), (70), takes into account mass transfer in the liquid phase represented by Eqs. (23)–(25) with the boundary conditions (29)–(31). In this model, the condition of 'flowing' across the phase boundary (30) is critical. In the case of $\rho > 1$ (for example, for a system of succinonitrile–acetone with $\rho = 1.028$), a strong interrelation occurs between the dynamic behaviour of the liquid phase and the dynamic behaviour of the interface. In other words, the condition (30) singularly perturbs the dynamic system (70), even when the relative density ρ is little different from one.

Then, sequentially executing all the operations as in the models considered above, one obtains a variance equation of order nine

$$\sum_{j=0}^{9} Q_{9-j} \cdot \Omega^{9-j} = 0. \tag{71}$$

The coefficients Q_i, $i \in \{0, 1, \ldots, 9\}$ of the dispersion equation (71), due to their bulkiness, are not explicitly represented here. However, they can be obtained by following the algorithm described above. The variance equation (71) describes model #3.

5. Results of Numerical Calculations

Numerical studies have been carried out for the process of directional solidification of succinonitrile–acetone binary system (SCN–Ac) (see Appendix 3). The main characteristic parameters of the process are as follows: acetone concentrations at an infinite distance from the inter-face $c_0 = 0.2$ mol.%, characteristic solidification rate $W_0 = 10^{-6}$ m/s, characteristic temperature difference $\theta_0 = 0.259$ K (chosen such that the dimensionless latent heat of solidification is $\Lambda \sim 1$). The roots Ω_j of the dispersion Eqs. (63), (70), (71) were computed by the Laguerre method [19]. Note that these roots are the natural numbers of the considered boundary problem and are related to the eigenfrequencies ω_j by the ratio

$$\omega_j = i \cdot \left(\frac{\Omega_j^2}{4} - \frac{\rho^2 \cdot w^2}{4} - k^2 \right), \; j = 1, \ldots, n, \tag{72}$$

where n is the order of the corresponding dispersion equation.

5.1. Model #1

Consider the results of the calculation of the spectral characteristics of the imaginary part of eigenfrequencies obtained by computing the roots of the dispersion equation (63) on some set of parameter values $\{\zeta, w\}$. Figure 2 shows the results of the spectral characterization of genera-lized increment $\delta_m(k)$ using the ratio (62). Three values of parameter
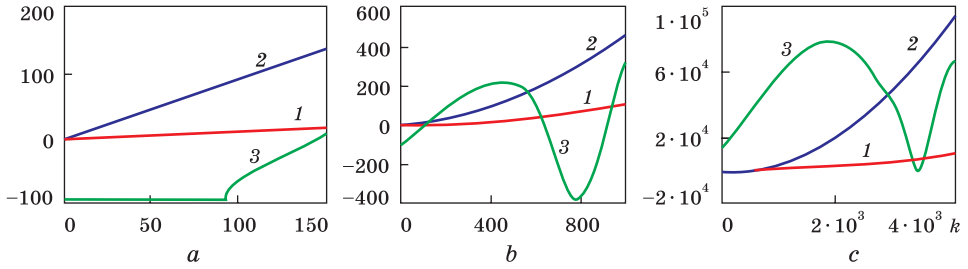
Fig. 2. Spectral characteristics of the increment $\delta_{m,i}(k)$, $i \in \{1, ..., 3\}$ obtained as a result of solving the second-order dispersion equation for $\zeta = 0.1291$ (*a*), $\zeta = 1.0$ (*b*), and $\zeta = 1.5$ (*c*). Curves *1*, *2*, and *3* correspond to the solidification rates $w = 0.01$, 1.0, and 100 respectively. Scale: (*a*) curve *1* — $\delta_{m,1}(k) \cdot 10$, *2* — $\delta_{m,3}(k)$; *3* — $\delta_{m,3}(k) \cdot 10^{-2}$; (*b*) curve *1* — $\delta_{m,1}(k) \cdot 2$, curve *2* — $\delta_{m,2}(k) \cdot 2$, curve *3* — $\delta_{m,3}(k) \cdot 0.5$; (*c*) — all curves scaled one to one
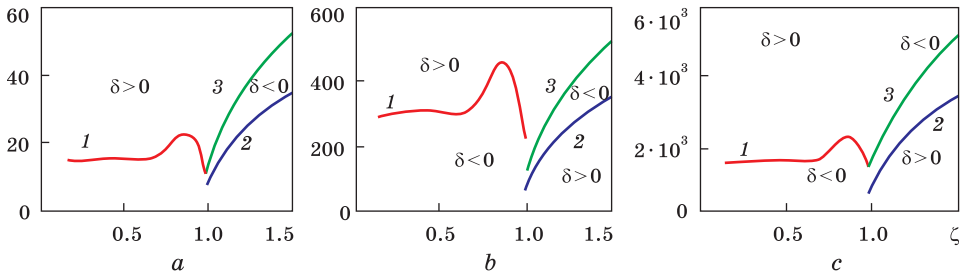
Fig. 3. Neutral stability curves (values k turning to zero increment: $\delta_m(k) = 0$ on the plane (k, ζ). Here, $w = 0.01$ (*a*), $w = 1.0$ (*b*), and $w = 100$ (*c*). Scale: *a* — (*1*) $k \cdot 10^3$, (*3*) $k \cdot 1.5$; *b* — (*1*) $k \cdot 2 \cdot 10^2$, (*3*) $k \cdot 1.5$; *c* — (*1*) $k \cdot 10$, (*3*) $k \cdot 1.5$

ζ ((20)−(22)) $\in \{0.1291; 1.0; 1.5\}$ and three values of solidification rate $w \in \{0.01; 1.0; 100.0\}$ were used. The figure shows that in the vicinity of the $k \sim 10^{-6}$ wavenumbers there is an area of stability ($\delta_m(k) < 0$), which expands as the solidification rate w increases for all $\zeta < 1$ values (Fig. 2, *a*, *b*). At $\zeta \geq 1$, as the velocity of w increases, the area of stability in the vicinity of small values of k disappears (Fig. 2 *c*, curve *3*). In other words, there is instability relative to the long wave perturbations, whereas stability area occurs under large k values. Then, as w increase, this area of stability expands and its borders move towards large values of k (short waves). Figure 3 represents neutral stability curves in the plane (k, ζ) (denoted by numbers *1*, *2*, *3*) for three solidification rates $w \in \{0.01; 1.0; 100.0\}$, which correspond to Fig. 3, *a*−*c*. Curve *1* encompass the stability area relative to the spatial perturbations in the long-wave part of the spectrum range of the values of the parameter ζ $\{0 < \zeta < 1\}$. In the range of values of $\zeta \in \{\zeta > 1\}$, the area of stability is placed between neutral stability curves *2* and *3*. As the solidification
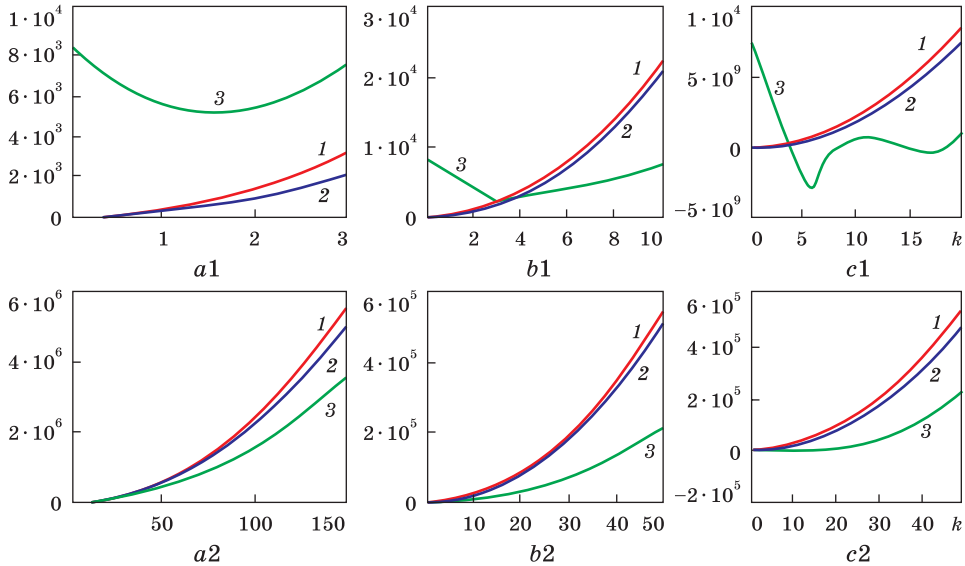
Fig. 4. Spectral curves of $\delta_{m,i}(k)$, $i \in \{1, ..., 3\}$ obtained as a result of the third order dispersion equation solution: $\zeta = 0.1291$ (*a1*, *a2*), $\zeta = 1.0$ (*b1*, *b2*), $\zeta = 1.5$ (*c1*, *c2*). Curves *1*, *2*, and *3* correspond to solidification rates $w = 0.01$, 1.0, and 100, respectively. Curve *1* (*a1*, *a2*) is constructed at the scale $\delta_{m,1}(k) \cdot 1.1$
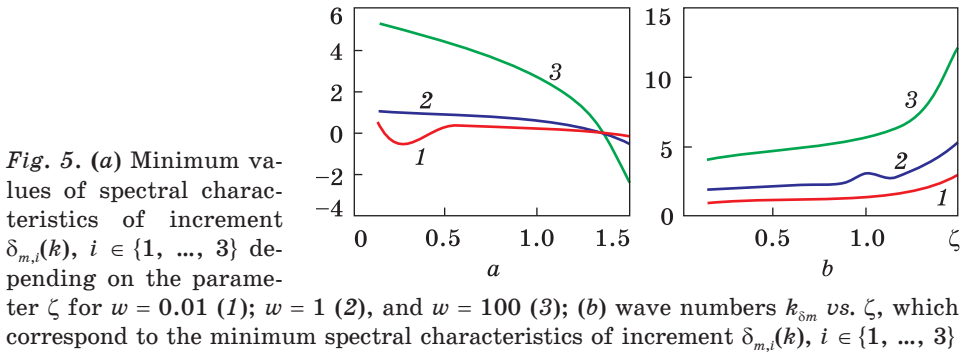

Fig. 5. (*a*) Minimum values of spectral characteristics of increment $\delta_{m,i}(k)$, $i \in \{1, ..., 3\}$ depending on the parameter ζ for $w = 0.01$ (*1*); $w = 1$ (*2*), and $w = 100$ (*3*); (*b*) wave numbers $k_{\delta m}$ *vs.* ζ, which correspond to the minimum spectral characteristics of increment $\delta_{m,i}(k)$, $i \in \{1, ..., 3\}$

rates increases, the neutral stability curves $\delta_{m,i}(k) = 0$, $i \in \{1, 2, 3\}$ move towards short waves (large values of k).

5.2. Model #2

Figure 4 shows the results of computing the spectral characteristics of the imaginary part of the roots of the dispersion equation (70) on a set of parameter values $\{\zeta, w\}$, which, according to the ratio (62), make it possible to compute the spectral characteristic of the generalized increment $\delta_m(k)$. Calculations show that the spectral characteristic $\delta_m(k)$, at some $k = k_m$ assumes a minimum value of $\delta_m(k_m)$. This value as well as
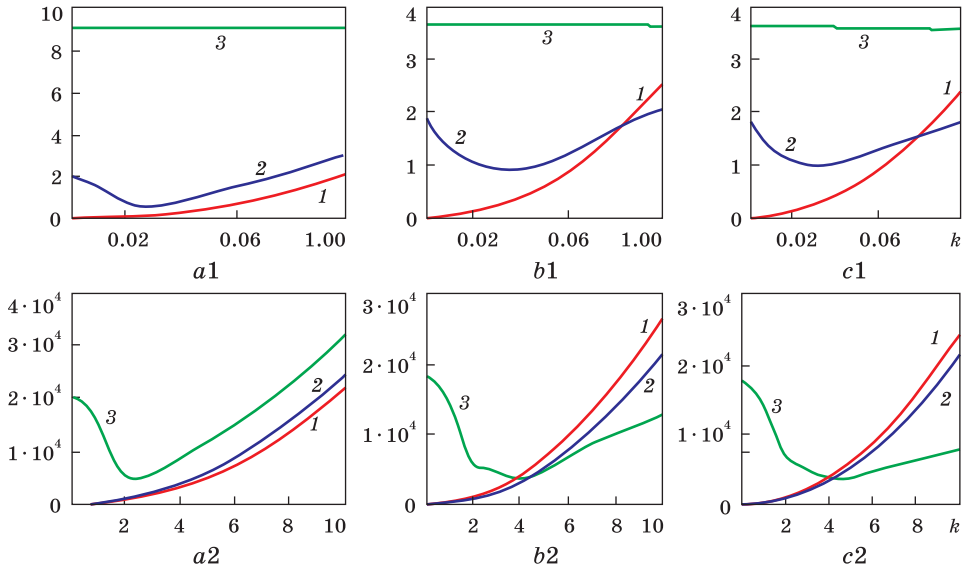
Fig. 6. Spectral characteristics of the generalized increment $\delta_{m,i}(k)$, $i \in \{1, ..., 3\}$ obtained as a result of solving the ninth-order dispersion equation. Here, $\zeta = 0.1291$ (*a*1, *a*2), $\zeta = 1.0$ (*b*1, *b*2), and $\zeta = 1.5$ (*c*1, *c*2). Curves *1*, *2*, and *3* correspond to the solidification rates $w = 0.01$, $w = 1.0$, and $w = 100$, respectively. Scale: (*a*1) curve $2 — \delta_{m,2}(k) \cdot 1.1$; $3 — \delta_{m,3}(k) \cdot 5 \cdot 10^{-4}$; (*a*2) curves 2 and $3 — \delta_{m,i}(k) \cdot 1.1$ for $i = 2, 3$; (*b*1) curve $3 — \delta_{m,3}(k) \cdot 2 \cdot 10^{-4}$; (*c*1) curve $3 — \delta_{m,3}(k) \cdot 2 \cdot 10^{-4}$; (*c*2) curve $1 — \delta_{m,1}(k) \cdot 1.1$

k_m wavenumbers is strongly dependent on the parameter ζ and the solidification rate w. In Figure 4, spectral characteristics are given for three values of parameter ζ and three values of solidification rate w (see signature to Fig. 4). Figures 4, 5 shows that at a fixed value of $\zeta < 1.3458$, as the speed w increases, the increment value of $\delta_m(k)$ increases at a value of $k \sim 10^{-6}$ (Fig. 5, *a*). Besides, the value of the minimum spectral characteristic of the increment $\delta_m(k_m)$ is increasing, as well as the wave numbers corresponding to the minimum of this spectral characteristic (Fig. 5, *b*). When $\zeta > 1.3458$, the opposite effect occurs: as w increases, the value of the minimum spectral characteristic of the increment $\delta_m(k_m)$ drops and becomes $\delta_m(k_m) < 0$ (Fig 5 *a*). So at $\zeta = 1.5$ and $w = 100$ one has a stable area: $\delta_m(k) < 0$ at $k \{3.861 < k < 8.154\}$ (Fig. 4, *c*1). As follows from Fig. 4, *a*2, *b*2, *c*2, for $k \in \{k > 20\}$, $\delta_{m,i}(k) > 0$ with $i \in \{1, 2, 3\}$.

5.3. Model #3

Model #3 assessed the impact of the density change and latent heat of solidification, along with the effect of concentration supercooling on interface stability. To this end, the spectral characteristics of the generalized increment $\delta_m(k, w)$ generated by the Ω_i roots of the dispersion equation (71) according to the ratios (60), (62) were studied. The results
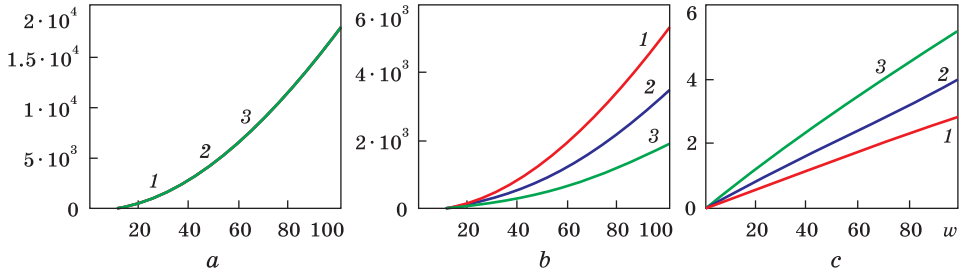
Fig. 7. The increment $\delta_{m,i}(w, k)$ and wave numbers $k\delta_{m,i}(w)$ corresponding to its minimum *vs.* the solidification rate. Curves *1*, *2*, and *3* correspond to $\zeta = 0.1291$, 1.0, and 1.5, respectively. (*a*) Dependence of the increment $\delta_{m,i}(w; k_0)$, $i \in \{1, ..., 3\}$, $k_0 \sim 10^{-6}$. (*b*) Dependence of minimum values of the increment $\delta_{m,i}(w; k_{\delta m,i}(w))$, $i \in \{1, ..., 3\}$. (*c*) Dependence of the wave numbers $k_{\delta m,i}(w)$, $i \in \{1, ..., 3\}$
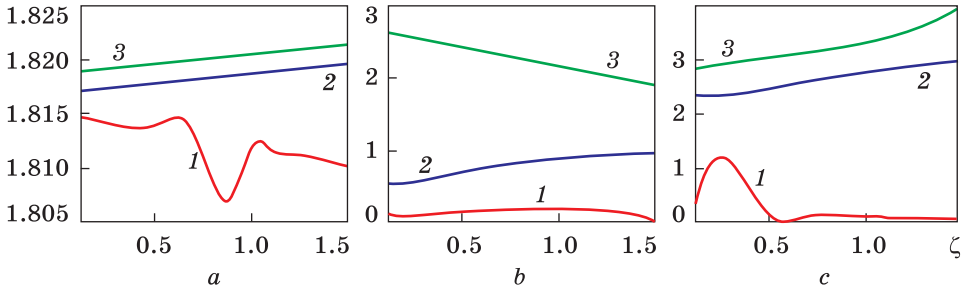

Fig. 8. The dependences of the increments $\delta_{m,i}(w, k)$ and wave numbers $k_{\delta m,i}(\zeta)$, corresponding to the minimum of the increment, on the parameter ζ. Curves *1*, *2*, *3* correspond to $w = 0.01$, 1.0, 100. (*a*) The dependence of increment $\delta_{m,i}(w, k)$, $i \in \{1, ..., 3\}$, $k_0 \sim 10^{-6}$; scale: $\delta_{m,1} \cdot 10^4$; $\delta_{m,2} \cdot 0.99$; $\delta_{m,3} \cdot 10^{-4}$. (*b*) The dependence of the minimum values of the increment $\delta_{m,i}(\zeta; k_{\delta m,i}(\zeta))$, $i \in \{1, ..., 3\}$; scale: $\delta_{m,1} \cdot 10^3$; $\delta_{m,3} \cdot 0.5 \cdot 10^{-4}$. (*c*) The dependence of wave numbers $k_{\delta m,i}(w)$, $i \in \{1, ..., 3\}$, $i \in \{1, ..., 3\}$; scale: $\delta_{m,1} \cdot 10^3$; $\delta_{m,2} \cdot 0.8 \cdot 10^2$

are shown in Figs. 6–8. Figure 6 demonstrates that the spectral characteristics of generalized increments $\delta_{m,i}(k)$, $i \in \{1, ..., 3\}$ have a minimum, which, with the increase of parameters w and ζ shifts towards the higher values of the wave numbers k_m. At the same time for $k > k_m$, there is a monotone increasing of $\delta_{m,i}(k)$, $i \in \{1,... ,3\}$ at $k \to \infty$. As the solidification rate w increases, the increasing rate of increment decreases $\delta_m(k)$, $k \to \infty$ (Fig. 6, *c2*). Figure 7 represents the w-dependent increments $\delta_{m,i}(w; k_0)$, $k_0 \sim 10^{-6}$ (Fig. 7, *a*), minimum increments $\delta_{m,i}(w; k_{\delta m,i}(w))$ (Fig. 7, *b*) and wave numbers $k_{\delta m,i}(w)$ corresponding to the minimum spectral characteristics of the increments for the three values ζ (Fig. 7, *c*). It can be seen from the figure that, with the increasing of w, the increment, at a given very small wavelength number $k = k_0$, monotonically grows and does not depend on the parameter ζ. Figure 8 shows the dependencies of the increments $\delta_{m,i}(\zeta; k_0)$, $\delta_{m,i}(\zeta; k_{\delta m,i}(\zeta))$ and wavenum-

bers $k_{\delta m,i}(\zeta)$ on the parameter ζ for the three values of the solidification rate (curves $i = 1$; 2; 3). At low solidification rates $w = 0.01$, the increment $\delta_{m,1}(\zeta; k_0)$ is slowly decreasing, if ζ increases (curve *1*, Fig. 8, *a*). At mean and sufficiently high solidification rates $w \in \{1.0; 100\}$, increment $\delta_{m,i}(\zeta; k_0)$ increases slightly under increasing of ζ (curve *2*, *3*, Fig. 8, *a*). The minimum value of increment $\delta_{m,i}(\zeta; k_{\delta m,i}(\zeta))$ decreases significantly, as the ζ increases and the solidification rates are high enough ($w = 100$; Fig. 8, *c*, curve *3*).

6. Discussion

The phenomenological approach developed in this paper allows studying the relative contribution of various physical effects to the loss of stability of a planar solid–liquid interface. It is known that the most approaches to this problem ignore such factors as the removal of latent melting heat through solid and density change during crystallization. The description of the latter factor allows clarifying the role of melt flow in the formation of interface morphology. The effect of melt flow caused by convection or forced stirring has been investigated in many studies (see references in [13]). For example, the work [9] shows that the flow can both suppress and stimulate the development of distortions on the interface. The analysis in Ref. [13] showed that the fluid flow tangent to the interface significantly reduces the areas of stability. Present paper examines the flux effects associated with a density change. This effect is irreducible because it is related to the internal properties of the substance. It is interesting to compare this effect with others that determine the loss of stability conditions at the interface during directional crystallization.

In order to solve the problem, the phenomenological theory of continuous media [19, 20] considers the hierarchy of three mathematical models of different complexity constructed in an infinite region of flat geometry. Furthermore, the stability of the phase boundary during the stationary process of directional solidification described by the system of Eqs. (1)–(11) is solved numerically. Stability conditions are investigated by introducing infinitely small perturbations followed by the determination of the generalized spectral characteristic (increment) $\delta_m(k, w)$, the sign of which defines areas of stability or instability. That is, the approach is basically same as in the theory of Mullins and Sekerka [6]. However, a substantial difference is the way of calculation the value of the temperature gradient at the interface. Theory [6] assumes the special temperature conditions on the heater and cooler that are necessary to form a stationary temperature gradient at the interface. In the presented model, it is assumed that the temperature of the heater and cooler at infinity have constant values ϑ_l and ϑ_s. The temperature gra-

dient at the crystallization front is described by two dimensionless parameters ζ and τ, whose values according to (21) and (22) are uniquely related to ϑ_l and ϑ_s, which automatically fulfil the stationary condition (17). In other words, the study of the stability of the crystallization front using ζ and τ is guaranteed for the stationary process described by Eqs. (1)−(11).

Note that the parameter τ, which is related to physical parameters by the ratio (19), at fixed values of w, l_t and ζ, determines the temperature of ϑ_s (22) and does not affect the stability of the crystallization front.

For ease of comparison of the results of all three models, the calculations were performed using a set of parameter values $\{\zeta, w\}$ common to the models in question.

Model #3 provides for the most complete consideration of factors controlling the real solidification process. In this case, the decisive role of the density change in comparison with other factors has been demonstrated, as well as the absence of the area of stable interface morphology. At the same time, it is interesting not only this end result, but also the evolution of the morphological features of the interface, taking into account different approximations. Note also that the present approach gives not only the configuration of the areas of stable interface morphology, but also allows to estimate the relative rates of the development of distortions of different wavelengths.

A comparison of the various approximations makes it possible to analyse the summary of results in Figs. 2−8. Model #1 (Figs. 2, 3) takes into account the transport of heat and impurity in a liquid phase, continuity equations for impurity flux crossing the phase boundary, and boundary conditions corresponding to the Mullins and Sekerka model. The calculated configurations of the stability areas demonstrate their alternation with the areas of instability in a wide range of solidification parameters. Figures 2, *a*, *b*, and 3 show that at $\zeta < 1$ and low k values the model #1 gives an area of stability that is missing when considering models ##2 and 3. There is a parameter range where this model gives a picture similar to that considered in Mullins and Sekerka theory. In Figure 2, *b*, we can see the emergence of a stability area at mean k values for some growth rate. In this case, numerical values have the same order of magnitude, with estimates made based on the theory [6] for the system of succinonitrile−acetone.

Additional consideration of latent melting heat in model #2 and mass transfer effect due to density change in model #3 (in addition to model #1) results in significant reconfiguration of the stability areas. Particularly, model #2 gives a weak instability $\delta_m = 10^{-5}$ for $w = 0.01$ and $\zeta = 0.1291$ (at $k = 10^{-6}$), which increases rapidly with w and ζ and at $w = 100$, $\zeta = 1.5$ reaches values of $\delta_m = 10^4$ (Fig. 4, *a*1−*c*1). Model #3 with increasing of w gives an even larger increase of instability at

$k = 10^{-6}$ (Fig. 6), which, in this model, is practically independent of the parameter ζ (Fig. 7, *a*). Thus, in models #2 and #3 (as opposed to model #1), at low values w, the front has a low instability relative to longwave perturbations, which increases rapidly with the solidification rate. Characteristically, the maximum contribution to long-wave instability is the effect of a density change on the solidification front.

The configuration of the obtained instability domains is characterized by pronounced extremes in the area of certain values of solidification parameters. For example, for model #1 at $\zeta = 1$ (in model #2, $\zeta = 1.3$), a special point is identified where all regions of stability and instability converge. At this point, the generalized increment $\delta_m(k, w)$ takes the minimum (for models #1 and #2 negative) values, which corresponds to the absence of perturbations (or their slow development in the case of model #3) for all growth rates. The observed features indicate that in the real spectrum of disturbances one should expect a large set of different frequencies which evolve at different speeds.

In order to compare present results with those of the experimental studies, one took the work [19] as reference one. First, it dedicated to experimental study of the interface dynamics during directional solidification of succinonitrile−acetone binary system, the physical characteristics of which are taken as a basis in present paper. In addition, the parameters of the experimental set-up and the measurement procedure are sufficiently detailed in Ref. [21]. To adapt our calculations to Ref. [21], in the co-ordinate system related to the solidification front, one enters the co-ordinate of the lower edge of the heater (Fig. 1):

$$z_h = l_h - l_t, \tag{73}$$

where l_h is the distance between the top edge of the cooler and the bottom edge of the heater (Fig. 1). Then, the temperature on the lower edge of the heater, considering (13), will have the following appearance

$$\theta_l(z_h) = \vartheta_l \cdot [1 - e^{-P_l \cdot w \cdot (l_h - l_t)}] + \vartheta_0 \, e^{-P_l \cdot w \cdot (l_h - l_t)} \tag{74}$$

and the temperature at the top of the cooler

$$\theta_s(-l_t) = \vartheta_s. \tag{75}$$

Solving Eq. (21) with respect to ζ and taking into account (74), one get

$$\zeta = -\frac{\chi P_l(\theta_h - \theta_0) + \Lambda^*[1 - e^{-P_l \, w(l_h - l_t)}]}{(1 - \kappa)\vartheta_0[1 - e^{-P_l \, w(l_h - l_t)}]}. \tag{76}$$

Note that, in this case (due to fixing the temperatures of the heater and the cooler and, therefore, the external gradient), parameter ζ becomes dependent on the solidification rate w. After deleting from (22) the parameter ζ, considering (75), and entering the symbol

$$x = e^{P_l w l_t}, \tag{77}$$

one gives an equation to determine the position of the solidification front l_t at fixed temperatures of heater $\vartheta_l(z_h) = \vartheta_h$ and cooler $\vartheta_s(-l_t) = \theta_c$.
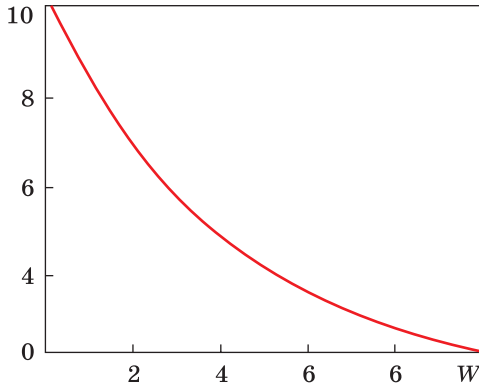
Fig. 9. Dependence of the interface position on the solidification rate under experimental conditions given in Ref. [10]
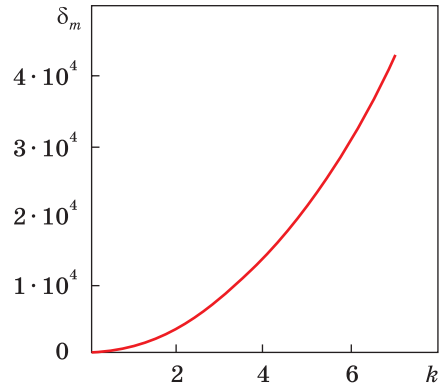
Fig. 10. Spectral characteristic of the increment $\delta_{m,i}(w, k)$ calculated for experimental conditions given in Ref. [10]

$$Ax^{1+\frac{P_s}{P_l}} + B_1 x + B_2 x^{\frac{P_s}{P_l}} + C = 0, \tag{78}$$

where

$$A = \Lambda^* \exp(-P_l w l_h),$$

$$B_1 = \left[\frac{P_s}{1-\kappa}(\theta_c - \vartheta_0) - \Lambda^*\right]\exp(-P_l w l_h),$$

$$B_2 = -\chi P_l(\theta_h - \theta_0) - \Lambda^*,$$

$$C = \chi P_l(\theta_h - \vartheta_0) - \frac{P_s}{1-\kappa}(\theta_c - \vartheta_0) + \Lambda^*.$$

Figure 9 shows the dependence $l_t(w)$ obtained from the solution of equation (78) for a set of w values. The experimental parameters from the work [21] used in the calculations are presented in Appendix 3.

Figure 10 shows the spectral characterization of the increment $\delta_m(k)$, calculated using a model adapted to Ref. [21] for the solidification rate of $w = 0.75$ μm/s. In order to get the relationship between $\delta_m(k)$ and the parameters characterizing the evolution of interface disturbances, one represents the interface disturbances function $\delta f_N(\xi, t)$ in the following way. Consider a superposition of N eigenfunctions of the boundary problem, which correspond to a set of unstable eigenvalues

$$\delta_m(n) = \delta_{m,n}, \ n \in \{0, 1, \dots, N\},$$

$$\delta f_N(\xi, t) = C_N \sum_{n=0}^{N} \frac{\sqrt{2}}{n+1} \exp[\delta_{m,n} \cdot \theta_n(t)] \cdot \cos\left[2\left((n+1)\pi\xi - \frac{\pi}{4}\right)\right], \tag{79}$$

where C_N is a normalizing constant, n is an integer wave number related to wave number k by the following ratio
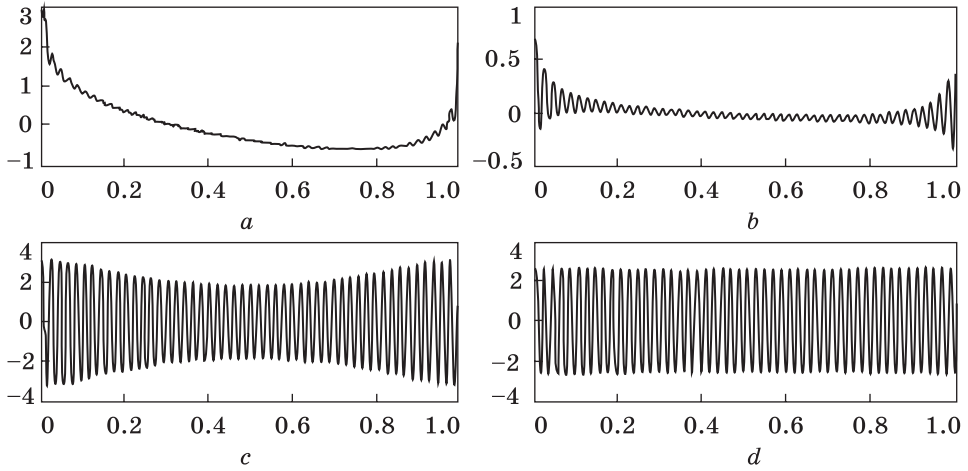
Fig. 11. Spatial structures formed as a result of superposition of 50 eigenfunctions corresponding to a set of unstable eigenvalues $\delta_m(n) = \delta_{m,n}$ ($n \in \{0, 1, ..., 49\}$) for time points $t = 2\cdot10^{-5}$ (*a*), $t = 1\cdot10^{-4}$ (*b*), $t = 1\cdot10^{-3}$ (*c*), $t = 3\cdot10^{-3}$ (*d*)

$$n - \left\lfloor k \cdot \frac{L_g}{L_0} \right\rfloor = 0, \quad n \quad \{1, 2, ..., N\}. \tag{80}$$

The latter takes place due to the finite interface length L_g. Then, solving Eq. (80) relative to the wave number k for each value $n \in \{1, 2, ..., N\}$, one gets a set of values of the wave numbers k_n. These values, according to the spectral characteristic (Fig. 10), determine the Eigen numbers (increments) $\delta_{m,n} = \delta_m(k_n)$, which are responsible for the development of the initial perturbation of the interface. The length of the interface L_g and the characteristic (diffusion) length L_0 are given in Appendix 3. Function $\lfloor \cdot \rfloor : x \to \lfloor x \rfloor$ is defined as the largest integer, less than or equal to x [22]. The function $\vartheta_n(t))$ (used in (79)) is defined as

$$\theta_n(t) = \begin{vmatrix} t \text{ if } t \leq T_n \\ T_n \text{ otherwise} \end{vmatrix} \tag{81}$$

with t being a dimensionless time,

$$T_n = \frac{3n}{\delta_{m,n}}. \tag{82}$$

Figure 11 displays the superposition $N + 1 = 50$ eigenfunctions (79) in the domain of ξ $\{0,1\}$, corresponding to the length of the interface $L_g = 0.01$ m, at times $t \in \{2\cdot10^{-5}; 10^{-4}; 10^{-3}; 3\cdot10^{-3}\}$. The structures presented in the figure are the result of superposition of eigenfunctions. Since a linear model was used, these structures should be considered the beginning of a process that becomes non-linear over time.

The structure presented in Fig. 11 is close to the cellular, and its period is close to the experimental one [21]. Therefore, it can be argued that the theory gives a qualitatively consistent with the experiment morphology of the interface. It should be noted that theory considers a linear model; so, the coincidence of the order of magnitude of the cellular spacing refers to the linear stage of patter formation. In most experiments known to us, as in the work [21], there is a substantially nonlinear process of cell formation, the description of which goes beyond this work.

7. Conclusions

The phenomenological analysis of the directional solidification of binary alloy, which account the influence of a solid–liquid density change and heat removal through solid phase has been developed for the problem of planar interface stability. The approach is free of some assumptions of Mullins and Sekerka theory, in particular the assignment of special conditions for the formation of a stationary temperature gradient at a crystallization front. The areas of stability and instability are described in terms of the system of parameters ζ and τ, whose range of values is guaranteed to provide the stationarity condition at the interface. They are only related to the temperature values of the heater and cooler (ϑ_l and ϑ_s).

The problem of interface stability was studied by introducing infinitesimal perturbations, followed by determination of eigenvalues of the boundary problem formulated for perturbations. The dispersion equation, which relates the wave number k to the complex frequency ω, is obtained in the form of a polynomial of degree n. Polynomial roots make their natural complex frequency ω dependent on the wave number and physical parameters of the solidification process. The sign and numerical value of the imaginary part of the complex frequency ω determines the index of increase ('+' increment) or attenuation ('−' decrement) of the amplitude of perturbations over time. The generalized spectral characteristic of the perturbation (increment) $\delta_m(k, w)$ is introduced, the sign of which is guaranteed to determine the areas of stability or instability of an interface.

Within the framework of the general approach, the hierarchy of three particular models, which correspond to different degrees of consideration of physical parameters of solidification process, has been studied. The model #1 (polynomial degree $n = 2$) takes into account of heat and impurity transfer in the liquid phase, condition for impurity flow continuity when crossing the phase boundary and boundary conditions, which correspond to Mullins and Sekerka model. Additional consideration of the latent melting heat in model #2 results in an increase

in the order of the dispersion equation to $n = 3$. Model #3 ($n = 9$) takes account of the liquid-phase mass transfer due to the effect of fluid movement due to density change other than the parameters included in models ##1 and 2.

Model #1 shows alternating areas of stability and instability over a wide range of solidification parameters. There is an interval of parameters where this model gives a similar behaviour as described in Mullins and Sekerka theory (Fig. 2, *b*): the emergence of stability area under mean K values for a certain growth rate value; the numerical values have one order of magnitude with the assessment of the theory [6] for the succinonitrile−acetone system. At the same time, in contrast to the Mullins and Sekerka theory, under relatively high growth rates and small K values, an area of stability has been identified.

For all models considered, there is a complex pattern of alternating areas of stability and instability, which is sensitive to the change of parameters w and ζ (dimensionless parameters characterizing the growth rate and temperature gradient at the interface). The configuration of the obtained areas includes pronounced extremes under certain values of solidification process parameters. Thus, for a model #1 at $\zeta = 1$ (in model #2, $\zeta = 1.3$), a special point is identified, in which all areas of stability and instability converge. At this point, the generalized increment $\delta_m(k, w)$ adopts minimum (in models ##1 and 2, it becomes negative) values, which corresponds to no perturbations (or their slow development in the case of model #3) for all growing rate values. The observed features indicate that in the real picture of perturbations development a large set of different frequencies that develop at different speeds should be expected.

A comparison of the three models shows that the effect of heat dissipation through the solid phase (model #2) and the melt flow due to the density change (model #3) has a significant influence on the occurrence of instability, and neglect of these factors distorts the physical picture of the process. The most significant factor in comparison with others is the density change at crystallization. When this factor is taken into account, there are no areas of stability, but only slowly developing long-wave distortions at low growth rates.

Comparison with the experiment demonstrates the relevance of the obtained picture of the development of unstable interface morphology

because of the interaction of perturbations of different wavelength. However, observation of an undistorted planar surface for a relatively long time can be explained by the long-term nature of long-wave disturbances at low growth rates.

<div align="right">*APPENDIX 1.*</div>

General View of the Equations Describing the Directional Solidification Process in the Absence of External Forces

Generally, the dimensionless equations, which determine the dynamics of directional crystallization of the binary melt, in some simply connected spatial domain (under specified conditions at the outer boundary), in the absence of external volume forces, are in the following forms:

$$\frac{\partial \mathbf{v}}{\partial t} + \mathbf{v}\nabla\,\mathbf{v} - \rho\cdot w\frac{\partial \mathbf{v}}{\partial z} = -\nabla p + \frac{1}{Re}\,\Delta\mathbf{v}, \tag{A1.1}$$

$$(\nabla\mathbf{v}) = 0, \tag{A1.2}$$

$$\frac{\partial T_l}{\partial t} + \mathbf{v}\nabla\,T_l - \rho\cdot w\frac{\partial T_l}{\partial z} = \frac{1}{P_l}\,\Delta T_l, \tag{A1.3}$$

$$\frac{\partial C}{\partial t} + \mathbf{v}\nabla\,C - \rho\cdot w\frac{\partial C}{\partial z} = \Delta C, , \tag{A1.4}$$

$$\frac{\partial T_s}{\partial t}{}_l - w\frac{\partial T_s}{\partial z} = \frac{1}{P_s}\,\Delta T_s, \tag{A1.5}$$

where $\mathbf{v}$ is vector of liquid flow velocity; w is the solidification rate (Fig. 1); p is a liquid phase pressure; T_l is liquid phase temperature; C is mass fraction of impurity in the liquid phase; T_s is solid phase temperature; $\mathbf{r}$ is vector in the coordinate space $\{x, y, z\}$; t is time. Diffusion in the solid phase is not considered.

The set of equations (A1.1)–(A1.5) should be supplemented with conditions for continuity of the flows across the interface [20]:

$$(\mathbf{v_n} - \mathrm{D}) = -\rho \mathrm{D}, \tag{A1.6}$$

$$P_\mathbf{n} + P_\mathbf{n} + \mathbf{v}(\mathbf{v}_n - \mathrm{D}) = P_{s,\mathbf{n}}, \tag{A1.7}$$

$$Me\,(R_\mathbf{n}\cdot\mathrm{D}) + Pp\,(P_\mathbf{n}\cdot\mathbf{v}) + \chi q_{l,\mathbf{n}} + [\Lambda + E_\mathbf{n}\cdot U_l](\mathbf{v_n} - \mathrm{D}) =$$

$$= q_{s,\mathbf{n}} - E_w\cdot\rho U_s\mathrm{D}, \tag{A1.8}$$

$$C_l(\mathbf{v_n} - \mathrm{D}) - (\mathbf{n}\cdot\nabla C_l) = -\rho\cdot C_s\,\mathrm{D}, \tag{A.1.9}$$

$$C_s = \kappa\cdot C_l, \tag{A1.10}$$

where v_n is the projection of the liquid phase velocity vector to the

positive normal direction $\mathbf{n}$; R_n is the surface density of the external forces distribution for the force medium (including surface tension); P_n is the surface density of internal forces; $q_{l\mathbf{n}}$ is projection of the specific heat energy flow from the liquid phase to the normal to the interface; $q_{s,\mathbf{n}}$ is projection of the flow of specific thermal energy in the solid phase to the normal to the interface; U_l is specific internal energy of the liquid phase; U_s is specific internal energy of solid; Λ is latent specific heat of melting; C_l is mass fraction of impurity at the interface on the liquid phase side; C_s is mass fraction of impurity at the interface on the solid phase side; κ is partition coefficient; v_n is velocity of the movement of the considered point r of the discontinuity surface $S(\mathbf{r}, t) = 0$ in the direction of the normal at that point. Here and further, index $\mathbf{n}$ means that this physical quantity is considered at the point of the discontinuity surface $S(\mathbf{r}, t) = 0$ with the norm with the normal $\mathbf{n}$.

Velocity vector $\mathbf{D}$ is represented by a ratio

$$\mathbf{D} = -\frac{\dfrac{\partial S}{\partial t}}{|\mathrm{grad}\ S|}\,\mathbf{n}_s, \tag{A1.11}$$

whereas the discontinuity surface is determined in this case by the ratio

$$S(\mathbf{r}', t) = z' - wt - h(x, y, t), \tag{A1.12}$$

where $h(x, y, t)$ is a deviation from the planar interface.

Ratios (A1.6)–(A1.10) represent the conditions for continuity of the flows across the interface of mass, momentum, energy and mass fraction of impurity, respectively [20].

Phenomenological relationship should be valid on the crystallization front:

$$T_l\big|_S = T_s\big|_S - B_m C_m - B_s \alpha \Delta_s h, \tag{A1.13}$$

where α is the dimensionless surface tension coefficient; Δ_s is Laplace operator on the surface S; T_M is melting point.

In the dimensionless reduction of the set of equations and boundary conditions, the following parameters were used as characteristic parameters: W_0 is solidification rate, $L_0 = D/W_0$ is length, $t_0 = D/W_0^2$ is time, θ_0 is temperature, and $C_{\infty, mol.\%}$ is molar concentration of impurity in the liquid phase at infinity.

Dimensionless complexes that are included in the system of equations (A1.1)–(A1.10), (A1.13) have the forms:

$$\boldsymbol{Re} = \frac{D}{\nu}, \quad P_s = \frac{D}{a_s}, \quad P_l = \frac{D}{a_l}, \quad B_p = \frac{\rho_l \cdot w_0^2 \cdot D}{\chi_s \Theta_0}, \quad \Lambda = \frac{\rho_l \cdot D \cdot \lambda}{\chi_s \Theta_0}, \quad B_m = \frac{m \cdot C_{\infty,\,mol\%}}{\Theta_0},$$

$$\chi = \frac{\chi_l}{\chi_s}, \ \rho = \frac{\rho_s}{\rho_l}, \ Mp = \frac{\alpha_0}{D \cdot w_0 \cdot \rho_l}, \ \alpha_C = \frac{\partial \alpha}{\partial C}\bigg|_{T=T_m}, \ \alpha_T = \frac{\partial \alpha}{\partial T}\bigg|_{C=J(0)}, \ c_{vl} = \frac{c_l}{c_0}, \ c_{vs} = \frac{c_s}{c_0},$$

$$Me = \frac{\alpha_0 \cdot w_0}{\chi_s \cdot \theta_0}, \quad E_w = \frac{\rho_l \cdot D \cdot c_0}{\chi_s}, \quad B_s = \frac{T_m \cdot w_0 \cdot \alpha_0}{\rho_l \cdot \lambda \cdot \Theta_0 \cdot D},$$

where ρ_1, υ are density and kinematic viscosity of liquid phase, respectively; a_l is thermal diffusivity of liquid phase; D is diffusion coefficient in the liquid phase; a_s is thermal diffusivity of solid phase; ρ_s is density of the solid phase; α_0 is surface tension coefficient; m is slope of the liquidus on the diagram of state; c_l, c_s are thermal capacities of the liquid and solid phases, respectively; λ is latent heat of melting.

Since Eqs. (A1.4), (A1.9), (A1.10) contain a mass fraction of impurity, and the phenomenological ratio (A1.13) contains a molar fraction of impurity, it is necessary to have a ratio that binds the molar and mass fraction of impurity:

$$C_{\text{mol\%}} = 100 \cdot C_{dm} \cdot C_m, \tag{A1.14}$$

where C_{dm} is the coefficient of normalization of the molar fraction C_m to unity at $z = \infty$. The molar fraction C_m is determined by the relation

$$C_m = \frac{n_a}{n_s + n_a}, \tag{A1.15}$$

where n_a is the amount of impurity moles (*e.g.*, acetone), n_s is the number of moles of the base substance.

The mass concentration of impurity is determined by the ratio

$$C_{\text{weidht\%}} = 100 \cdot C_{dw} \cdot C_w, \tag{A1.16}$$

where C_{dw} is the coefficient of normalization of the mass fraction C_w to unity at $z = \infty$. The mass fraction C_w is determined by the relation

$$C_w = \frac{n_a \cdot M_a}{n_s \cdot M_s + n_a \cdot M_a}, \tag{A1.17}$$

where M_a is molecular mass of the impurity, M_s is molecular mass of the basic substance.

From the ratios (A1.15), (A1.17), taking into account (A1.14), (A1.16), the ratio between molar and mass fractions of impurity is obtained as follows:

$$C_m(y, z, t) = \frac{\dfrac{C_{dw}}{C_{dm}} M_s C_w(y, z, t)}{M_a + C_{dw} C_w(y, z, t)(M_s - M_a)} \tag{A1.18}$$

where $C_m(y, z, t)$ is normalized molar fraction of impurity, C_{dw} is normalization factor to unit of mass fraction at infinity; C_{dm} is normalization factor to unit of molar fraction at infinity, $C_w(y, z, t)$ is normalized mass fraction of impurity, M_s is molecular mass of succinonitrile, M_a is molecular mass of acetone.

When passing to perturbations problem, it takes place as follow:

$$C_w(y, z, t) \rightarrow J(z) + \varepsilon C(y, z, t), \tag{A1.19}$$

$$C_m(y, z, t) \rightarrow J_m(z) + \varepsilon C_m(y, z, t), \tag{A1.20}$$

where $J(z)$, $J_m(z)$ are mass and molar fractions of impurity in the stationary process, respectively; $C(z, t)$, $C_m(z, t)$ are perturbations of mass and molar fractions of impurity, respectively. Replacing in (A1.18) the molar and mass fractions of impurity according to (A1.19) and (A1.20), we get

$$J_m(z) = \frac{\dfrac{C_{dw}}{C_{dm}} M_s J(z)}{M_a + C_{dw}(M_s - M_a)J(z)}, \tag{A1.21}$$

$$C_m(z, t) = \frac{\dfrac{C_{dw}}{C_{dm}} M_s M_a}{[M_a + C_{dw}(M_s - M_a)J(z)]^2} C(z, t). \tag{A1.22}$$

The relationship between the derivatives $J'_m(z)$ and $J'(z)$ has the form

$$J'_m(z) = \frac{\dfrac{C_{dw}}{C_{dm}} M_s M_a}{[M_a + C_{dw}(M_s - M_a)J(z)]^2} J'(z). \tag{A1.23}$$

Next, enter the symbol

$$B_w = \frac{\dfrac{C_{dw}}{C_{dm}} M_s M_a}{[M_a + C_{dw}(M_s - M_a)J(0)]^2} B_m. \tag{A1.24}$$

Then, taking into account (A1.22) and (A1.24), at the interface, the following ratios should be valid:

$$B_m J'_m(0) = B_m J'(0), \tag{A1.25}$$

$$B_m C_m(0, t) = B_m C(0, t). \tag{A1.26}$$

APPENDIX 2.

Explicit Form of the Functions Used in Eqs. (52)–(55)

$$\lambda_1 = -\frac{w}{2} + \sqrt{\frac{\rho_2 w^2}{4} + k^2 - i\omega}, \tag{A2.1}$$

$$\lambda_2 = -\frac{P_l \cdot \rho \cdot w}{2} + \sqrt{\frac{(P_l \cdot \rho \cdot w)^2}{4} + k^2 - i \cdot P_l \cdot \omega}, \tag{A2.2}$$

$$\lambda_3 = -\frac{P_s \cdot \rho \cdot w}{2} + \sqrt{\frac{(P_s \cdot \rho \cdot w)^2}{4} + k^2 - i \cdot P_s \cdot \omega}, \tag{A2.3}$$

$$f_1^c(z) \cong 1 + e^{-Re \cdot \rho \cdot w \cdot z}, \tag{A2.4}$$

$$f_2^C(z) \cong \frac{ik \cdot \beta_\kappa \cdot \rho \cdot w}{k \cdot \rho \cdot w + i\omega}, \tag{A2.5}$$

$$f_3^C(z) \cong \frac{ik \cdot \beta_\kappa \cdot \rho \cdot w}{k \cdot \rho \cdot w + i\omega} \left(z + \frac{\rho \cdot w + 2k}{k \cdot \rho \cdot w + i\omega} \right), \tag{A2.6}$$

$$f_1^t(z) \cong 1 + e^{-Re \cdot \rho \cdot w \cdot z}, \tag{A2.7}$$

$$f_2^t(z) \cong \frac{ik \cdot P_l \cdot \rho \cdot w (\vartheta_l - \vartheta_0)}{k \cdot \rho \cdot w + i\omega}, \tag{A2.8}$$

APPENDIX 3.

Parameters of the Experiment [21].
Thermophysical Properties of Succinonitrile−Acetone System

No.	Physical and Experimental Parameters	Value
1	Heater temperature, T_h	166 °C
2	Dimensionless temperature difference on the heater, $\vartheta_h = (T_h - T_m)/\vartheta_0$	416.641
3	Cooler temperature, T_c	16 °C
4	Dimensionless temperature difference on the cooler, $\vartheta_c = (T_c - T_m)/\vartheta_0$	−162.51
5	Distance between heater and cooler, L_h	0.05 m
6	Dimensionless distance between heater and cooler, $l_h = L_h W_0/D$	39.37
7	Temperature gradient, $G_e = (T_h - T_c)/L_h$	3000 °C/m
8	Dimensionless temperature gradient, $G_\vartheta = DG_e/W_0\vartheta_0$	14.71
9	Length of solidification front, L_g	0.01m
10	Dimensionless length of solidification front, $l_g = L_g W_0/D$	7.874
11	Characteristic (diffusion) length, $L_0 = D/W_0$	0.00127 m
12	Molar fraction of impurity at infinity, C_{dm}	0.002
13	Mass fraction of impurity at infinity, C_{dw}	0.00145

Succinonitrile Parameters	Value	Remarks
Molecular mass (M_{SCN})	80.092 g·mole⁻¹	—
Density of solid state (ρ_s)	1.016 g/cm³	Extrapolated to melting point
Density of liquid (ρ_m)	0.988 g/cm³	In melting point
Equilibrium melting point (T_m)	58.09 °C	—
Melting heat (λ)	3702.8 J·mole⁻¹	—
Specific heat in solid state (C_{ps})	153.21 J·mole⁻¹·K	In melting point
Specific heat in melted state (C_{pl})	160.18 J·mole⁻¹·K	In melting point
Thermal conductivity in solid state (k_s)	2.24·10⁻³ J·(cm·s·K)⁻¹	In melting point
Thermal conductivity in melted state (k_l)	2.23·10⁻³ J·(cm·s·K)⁻¹	In melting point
Free energy of the interface (α_{sl})	8.95·10⁻⁷ J·cm⁻²	In melting point

Properties of Succinonitrile−Acetone Melt	Value
Molecular mass (M_{ACE})	58.079 g·mole^{-1}
Diffusion coefficient (D)	1.27·10^{-5} cm^2/s
The slope of the liquidus line (m)	−2.22 °C/mol.%
Partition coefficient (κ)	0.1

$$f_3^t(z) \cong \frac{ik \cdot \rho \cdot w}{k \cdot \rho \cdot w + i\omega}\left(P_l \cdot z + \frac{P_l \cdot \rho \cdot w + 2k}{k \cdot \rho \cdot w + i\omega}\right), \qquad (A2.9)$$

where

$$\beta_\kappa \cong \frac{1 - \kappa}{\kappa}.$$

REFERENCES

1. M.C. Flemings, *Metall. Trans.*, **5**: 2121 (1974);
   https://doi.org/10.1007/BF02643923
2. A.A. Chernov, *Modern Crystallography III. Crystal Growth* (Berlin−Heidelberg: Springer: 1984);
   https://doi.org/10.1007/978-3-642-81835-6
3. W. Kurz and D.J. Fisher, *Fundamentals of Solidification, 4th Edition* (CRC Press: 1998).
4. *Materials Sciences in Space. A Contribution to the Scientific Basis of Space Processing* (Eds. B. Feuerbacher, H. Hamacher, and R.J. Naumann) (Berlin−Heidelberg: Springer: 1986);
   https://doi.org/10.1007/978-3-642-82761-7
5. V.I. Strelov, I.P.Kuranova, B.G. Zakharov, and A.E. Voloshin, *Crystallography Reports*, **59**, No. 6: 781 (2014);
   https://doi.org/10.1134/S1063774514060285
6. W.W. Mullins and R.F. Sekerka, *J. Appl. Phys.*, **35**, No. 2: 444 (1964);
   https://doi.org/10.1063/1.1713333
7. B. Caroli, C. Caroli, C. Misbah, and B. Roulet, *J. Physique*, **46**: 401 (1985);
   https://doi.org/10.1051/jphys:019850046030401000
8. N. Noel, H. Jamgotchian, and B. Billia, *J. Crystal Growth*, **181**, Nos. 1−2: 117 (1997);
   https://doi.org/10.1016/S0022-0248(97)00274-1
9. S.H. Davis and T.P. Schulze, *Metall. Mater. Trans. A*, **27**: 583 (1996);
   https://doi.org/10.1007/BF02648948
10. T. Jiang, M. Georgelin, and A. Pocheau, *EPL*, **102**, No. 5: 54002 (2013);
    https://doi.org/10.1209/0295-5075/102/54002
11. N. Noel, H. Jamgotchian, and B. Billia, *J. Crystal Growth*, **187**, Nos. 3−4: 516 (1998); https://doi.org/10.1016/S0022-0248(97)00882-8
12. H. Jamgotchian, N. Bergeon, D. Benielli, P. Voge, and B. Billia, *Microscopy*, **203**, No. 1: 119 (2001);

https://doi.org/10.1046/j.1365-2818.2001.00900.x

13. O.P. Fedorov and A.G. Mashkovskiy, *Crystallogr. Rep.*, **60**, No. 2: 236, (2015); https://doi.org/10.1134/S1063774515020091

14. S. Coriell, G. McFadden, W.F. Mitchell, B. Murray, J. Andrews, and Y. Arikawa, *J. Crystal Growth*, **224**, Nos. 1−2: 145 (2001); https://doi.org/10.1016/S0022-0248(01)00724-2

15. A. Mori, M. Sato, and Y. Suzuki, *Jpn. J. Appl. Phys.*, **58**, No. 4: 045506 (2019); https://doi.org/10.7567/1347-4065/ab0707

16. D. Oxtoby, *J. Chem. Phys.*, **96, No. 5**: 3834 (1992); https://doi.org/10.1063/1.462864

17. M. Conti, *Phys. Rev. E*, **64**, No. 5: 051601 (2001); https://doi.org/10.1103/PhysRevE.64.051601

18. M. Conti and M. Fermani, *Phys. Rev. E*, **67**, No. 2: 026117 (2003); https://doi.org/10.1103/PhysRevE.67.026117

19. L. Sedov, *Mechanics of Continuous Media* (World Scientific: 1997), vol. **2**; https://doi.org/10.1142/0712-vol2

20. L.D. Landau and E.M. Lifshitz, *Fluid Mechanics* (Pergamon Press: 1987).

21. T.C. Lee and R.A. Brown, *Phys. Rev. B*, **47**, No. 9: 4937 (1993); https://doi.org/10.1103/PhysRevB.47.4937

22. R. Graham, E. Knuth, and O. Patashnik, *Concrete Mathematics − A Foundation for Computer Science* (2nd Edition) (Addison-Wesley: 1994).

О.П. Федоров[1,2], *А.Г. Машковський*[1], *Є.Л. Живолуб*[2]

[1] Інститут космічних досліджень НАН України та ДКА України,
  просп. Академіка. Глушкова 40, корп. 4/1, 03187 Київ, Україна

[2] Інститут металофізики ім. Г.В. Курдюмова НАН України,
  бульв. Академіка Вернадського, 36, 03142 Київ, Україна

СТІЙКІСТЬ ФАЗОВОЇ МЕЖІ КРИСТАЛ−РОЗПЛАВ ПРОТЯГОМ СПРЯМОВАНОЇ КРИСТАЛІЗАЦІЇ: ФЕНОМЕНОЛОГІЧНА ТЕОРІЯ

Розроблено математичну модель, що уможливлює в межах єдиного феноменологічного підходу дослідити стійкість пласкої фазової межі протягом спрямованого твердіння двокомпонентного сплаву з урахуванням впливу стрибка густини на фазовій межі та тепловідведення через тверду фазу. Виявлено складну картину чергування областей стійкости та нестійкости, чутливу до зміни параметрів вирощування та температурного ґрадієнту на фронті кристалізації. Області нестійкости характеризуються великим набором частот збурень, що розвиваються з різними швидкостями. Показано, що неусувна течія рідкої фази, спричинена стрибком густини, відіграє головну роль у втраті стійкости фронту твердіння та реалізується для збурень з будь-яким хвильовим числом $k > 0$.

Ключові слова: двокомпонентний сплав, фазова межа кристал−розплав, спрямоване твердіння, морфологічна стійкість, стрибок густини, прихована теплота плавлення, дисперсійне рівняння.